

**ANNEALING OF ULTRA-SHALLOW IMPLANTED JUNCTIONS USING ARC-LAMP
TECHNOLOGY: ACHIEVING THE 90 NM NODE**

Robin Sarah Tichy¹, Kiefer Elliott², Steve McCoy², and David C. Sing¹

¹International SEMATECH
2706 Montopolis Drive
Austin, TX 78741

²Vortek Industries Ltd.
605 West Kent Avenue Vancouver
BC, Canada V6P 6T7

© 2000 IEEE. Personal use of this material is permitted. However, permission to reprint/republish this material for advertising or promotional purposes or for creating new collective works for resale or redistribution to servers or lists, or to reuse any copyrighted component of this work in other works must be obtained from the IEEE.

ANNEALING OF ULTRA-SHALLOW IMPLANTED JUNCTIONS USING ARC-LAMP TECHNOLOGY: ACHIEVING THE 90 NM NODE

Robin Sarah Tichy¹, Kiefer Elliott², Steve McCoy², and David C. Sing¹

¹International SEMATECH
2706 Montopolis Drive
Austin, TX 78741

²Vortek Industries Ltd.
605 West Kent Avenue Vancouver
BC, Canada V6P 6T7

This paper demonstrates the ability of extremely sharp spike anneals, used in combination with low energy implants, to achieve stringent source/drain junction requirements. The International Roadmap for Semiconductors imposes aggressive restrictions on the source/drain extension junction depth (X_j) and sheet resistance (R_s)¹. Spike annealing has been proposed as a process that can enable the realization of the 90nm node, which requires $X_j < 350\text{\AA}$ and $R_s < 650\text{ohm/sq}$. Very short thermal cycle times minimize dopant diffusion, and the arc-lamp system, developed by Vortek Industries Ltd., yields a significant reduction in the time within 50°C of the peak temperature. Recent experiments, which employed a variety of anneal temperatures and ramp rates, were conducted with two implants species; blanket wafers implanted with low energy B with Ge pre-amorphization (PAI) and BF_2 with and without PAI, were tested. Several implant/anneal combinations are shown to provide X_j/R_s values that fall well within the 90nm reference box.

INTRODUCTION

Shallow p⁺-n junction formation presents an obstacle to the scaling down of feature size in CMOS technology. Traditional ion-implant and rapid thermal processing cannot achieve the X_j/R_s values necessary because Boron implants have limited activation and non-equilibrium enhanced diffusion. Low energy implants confine defects close to the surface, minimizing the effects of defect-enhanced diffusion². Germanium pre-amorphization can prevent channeling and increase activation^{3,4}.

Relatively high peak anneal temperatures are necessary to activate the Boron; many studies have shown that a small thermal budget, or short cycle time within 50°C of peak, coupled with a high peak temperature minimizes the distance of dopant diffusion while allowing sufficient dopant activation⁵ and damage removal to achieve low sheet resistances. The water-walled arc-lamp system, developed by Vortek Industries Ltd., has superior lamp response time and spectral distribution. In addition, a black process chamber is used in order to limit radiation return

to the wafer and increase cooling rates. This results in faster, sharper spike anneal profiles than conventional tungsten lamp systems. This system enables the realization of a more idealized spike profile, and the limits of traditional implant and anneal processes can be explored. A large designed experiment (DOE) leads to the discovery of the specific conditions that will result in junction depths and sheet resistances that meet the specifications of the 90nm node.

The calculation of a thermal budget, defined as the square root of the integration of the time-temperature profile, allows the simultaneous evaluation of different anneal temperatures and ramp rates. A comparison of resulting junction depths to applied thermal budget provides evidence that shallow junctions are, in a large part, the result of very sharp spike profiles. Also, the energy required for the activation of the dopant is different than that required for diffusion. Therefore, an ideal peak temperature that minimizes diffusion and maximizes activation can be calculated for every dopant species. Unfortunately, reliable values for these

energies are generally unavailable, and the ideal processing temperature must be determined experimentally. The data obtained for the DOE presented in this work reveals optimum spike temperatures for B and BF₂ implants.

EXPERIMENTAL

The low energy B⁺, BF₂⁺ and Ge PAI implants were carried out on an Applied Materials XR-Leap implanter. The spike anneals were performed at Vortek Industries Ltd. with the arc-lamp system. The arc-lamp enables extremely fast ramp-up rates and a maximum cool-down rate of 150°C/s. A typical time-temperature profile is recorded in Figure 1. A variety of ramp-up rates and peak temperatures were explored, but all samples were processed

with a 0s dwell time and cooled at the maximum rate in Nitrogen ambient atmospheres.

The X_j and R_s values of blanket wafers were investigated for BF₂⁺ and B⁺ implant species. All B⁺ implanted wafers were pre-amorphized with Ge. The B⁺ and BF₂⁺ DOE's are four factor; implant energy, implant dose, temperature and ramp rate were varied. An attempt was made to optimize PAI energy and dose for each species. The details of the DOE are shown in Table I. The trends revealed prompted a second set of experiments targeting the 90nm technology node. In particular, it was evident that BF₂⁺ implants with Ge PAI could achieve optimal X_j/R_s values. Further exploration of the effect of ramp-up rate was necessary, also. The second experiment is detailed in Table II.

Table I: The Experimental Conditions

sample ID	PAI E	PAI Dose	Species	Energy [keV]	Dose	Temp. [C]	Ramp [C/s]	Rs [ohms/sq.]	Xj [1E18]
1 A 1	0	0	BF2	2	1.00E+15	1039.5	300	1110	244
1 B 1	0	0	BF2	2	1.00E+15	1139.0	300	404.3	411
1 D 1	0	0	BF2	2	1.00E+15	1039.2	500	1117	234
1 E 1	0	0	BF2	2	1.00E+15	1139.0	500	425.2	418
2 A 1	0	0	BF2	2	3.00E+15	1039.5	300	846.8	273
2 B 1	0	0	BF2	2	3.00E+15	1139.0	300	237.3	602
2 D 1	0	0	BF2	2	3.00E+15	1038.9	500	866.9	318
2 E 1	0	0	BF2	2	3.00E+15	1139.0	500	245.4	598
3 C 1	0	0	BF2	3	2.00E+15	1089.3	400	393.8	369
3 C 2	0	0	BF2	3	2.00E+15	1089.5	400	393.3	415
4 A 1	0	0	BF2	4	1.00E+15	1039.5	300	619	382
4 B 1	0	0	BF2	4	1.00E+15	1139.0	300	300.8	497
4 D 1	0	0	BF2	4	1.00E+15	1038.9	500	622.5	369
4 E 1	0	0	BF2	4	1.00E+15	1139.0	500	299.8	503
5 A 1	0	0	BF2	4	3.00E+15	1039.5	300	561.7	414
5 B 1	0	0	BF2	4	3.00E+15	1138.8	300	199.6	583
5 D 1	0	0	BF2	4	3.00E+15	1039.2	500	566.5	473
5 E 1	0	0	BF2	4	3.00E+15	1139.2	500	210.7	577
6 C 1	2	5.00E+13	BF2	3	2.00E+15	1089.3	400	398.4	339
7 C 1	2	2.00E+14	BF2	3	2.00E+15	1089.5	400	418.4	387
8 C 1	3.5	1.25E+14	BF2	3	2.00E+15	1089.0	400	422.1	386
8 C 2	3.5	1.25E+14	BF2	3	2.00E+15	1089.3	400	425.5	398
9 C 1	5	5.00E+13	BF2	3	2.00E+15	1089.5	400	403.3	361
10 C 1	5	2.00E+14	BF2	3	2.00E+15	1089.3	400	394.4	380
11 A 1	5	5.00E+14	B	0.5	1.00E+15	1039.5	300	826.2	308
11 B 1	5	5.00E+14	B	0.5	1.00E+15	1139	300	303.1	493
11 D 1	5	5.00E+14	B	0.5	1.00E+15	1038.9	500	840.8	302

11	E	1	5	5.00E+14	B	0.5	1.00E+15	1138.8	500	314.8	524
12	A	I	5	5.00E+14	B	0.5	3.00E+15	1039.5	300	619.6	327
12	B	1	5	5.00E+14	B	0.5	3.00E+15	1139.2	300	199.7	699
12	D	1	5	5.00E+14	B	0.5	3.00E+15	1039.2	500	644.5	279
12	E	1	5	5.00E+14	B	0.5	3.00E+15	1139	500	209.1	623
13	C	1	5	5.00E+14	B	0.75	2.00E+15	1089.3	400	301.3	467
13	C	2	5	5.00E+14	B	0.75	2.00E+15	1089.5	400	303.8	429
14	A	I	5	5.00E+14	B	1	1.00E+15	1039.5	300	571	329
14	B	1	5	5.00E+14	B	1	1.00E+15	1139	300	247.8	540
14	D	1	5	5.00E+14	B	1	1.00E+15	1039.2	500	565	328
14	E	1	5	5.00E+14	B	1	1.00E+15	1138.8	500	255.7	597
15	A	1	5	5.00E+14	B	1	3.00E+15	1039.5	300	418.1	467
15	B	1	5	5.00E+14	B	1	3.00E+15	1139	300	145.6	729
15	D	1	5	5.00E+14	B	1	3.00E+15	1039.2	500	425.3	417
15	E	1	5	5.00E+14	B	1	3.00E+15	1139.2	500	151.1	813
16	C	1	3	3.00E+14	B	0.75	2.00E+15	1089	400	355.7	442
<i>17</i>	<i>C</i>	<i>I</i>	<i>3</i>	<i>7.00E+14</i>	<i>B</i>	<i>0.75</i>	<i>2.00E+15</i>	<i>1089.3</i>	<i>400</i>	<i>432</i>	<i>375</i>
18	C	1	5	5.00E+14	B	0.75	2.00E+15	1089	400	304.9	467
18	C	2	5	5.00E+14	B	0.75	2.00E+15	1089	400	302.4	480
19	C	1	7	3.00E+14	B	0.75	2.00E+15	1089.5	400	298.3	461
20	C	1	7	7.00E+14	B	0.75	2.00E+15	1089	400	316.6	454

Table II: The Refined Experimental Conditions That Target the 90nm Technology Node

Sample ID	PAI E	PAI Dose	Species	Energy [keV]	Dose	Temp. [C]	Ramp [C/s]	Rs [ohms/sq.]	Xj [1E18]		
6	A	1	2	5.00E+13	BF2	3	2.00E+15	1071	100	451.1	373
6	B	1	2	5.00E+13	BF2	3	2.00E+15	1068.9	200	464.3	370
6	C	1	2	5.00E+13	BF2	3	2.00E+15	1070.7	300	489.2	363
6	D	1	2	5.00E+13	BF2	3	2.00E+15	1070.7	400	491.4	352
6	E	1	2	5.00E+13	BF2	3	2.00E+15	1071.6	500	511.9	372
10	A	1	5	2.00E+14	BF2	3	2.00E+15	1071	100	474.6	330
10	B	1	5	2.00E+14	BF2	3	2.00E+15	1070.1	200	532.2	316
10	C	1	5	2.00E+14	BF2	3	2.00E+15	1070.7	300	498.7	320
10	D	1	5	2.00E+14	BF2	3	2.00E+15	1070.7	400	500.6	335
10	E	1	5	2.00E+14	BF2	3	2.00E+15	1071.6	500	497.5	328
17	A	1	3	7.00E+14	B	0.75	2.00E+15	1038.9	400	779.1	296
17	B	1	3	7.00E+14	B	0.75	2.00E+15	1063.7	400	641.4	360
17	C	1	3	7.00E+14	B	0.75	2.00E+15	1088	400	458.2	420
12	A	1	5	5.00E+14	B	0.5	3.00E+15	1040	100	581.7	348
12	B	1	5	5.00E+14	B	0.5	3.00E+15	1040	200	581.7	351
12	D	1	5	5.00E+14	B	0.5	3.00E+15	1040	400	533	343
12	E	1	5	5.00E+14	B	0.5	3.00E+15	1040	500	586.7	327
14	A	1	5	5.00E+14	B	1	1.00E+15	1040.9	100	514.1	379
14	B	1	5	5.00E+14	B	1	1.00E+15	1039.9	200	550.5	379
14	C	1	5	5.00E+14	B	1	1.00E+15	1040.9	300	552	371
14	D	1	5	5.00E+14	B	1	1.00E+15	1040.3	400	558.5	373
14	E	1	5	5.00E+14	B	1	1.00E+15	1040.9	500	545.6	370

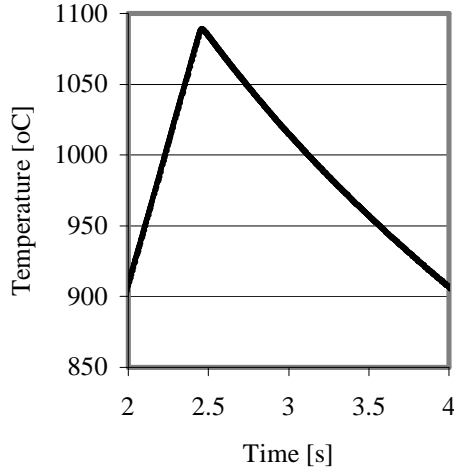


Figure 1: Spike anneal profile produced by arc-lamp technology.

RESULTS AND DISCUSSION

The X_j/R_s values obtained for each experimental condition are given in Tables I and II. The conditions that yielded a result that fell within the specifications of the 90nm technology node are in bold type. Figure 2 illustrates that this data shows a significant advancement to the lower right of the X_j/R_s array when compared with previously published data. The 90nm reference box is heavily populated by the BF_2^+ implants with Ge PAI. Two B^+ implant energy/dose combinations obtained the 90nm node, 1keV/1E15 and 0.5keV/3E15. Unfortunately, the 0.5keV/3E15, a non-ideal implant for routine production, routinely gave the better result.

It is clear from casual observation of the data that the ideal anneal temperature for the BF_2^+ implants with PAI is approximately 1070°C, and the optimized temperature for the B^+ implants is about 1040°C. The effect of temperature for BF_2^+ and B^+ implant species is illustrated by Figures 3 and 4, respectively. Temperature has the greatest effect on the post-anneal dopant depth.

The effect of ramp-up rate was not dramatic. The change in X_j and R_s values over a range of ramp rates is shown in Figure 5 for two BF_2^+ implant conditions. The changes were small for all implant/anneal combinations tested.

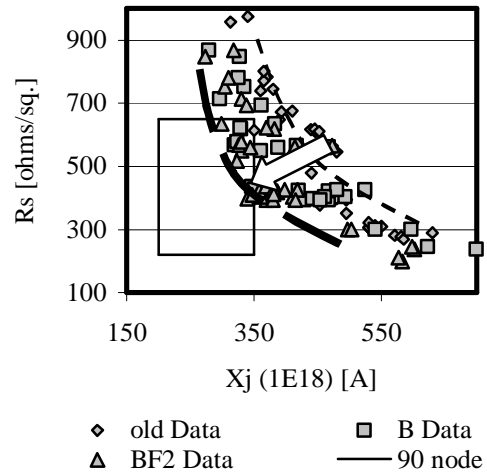


Figure 2: Current data compared to previous data obtained from spike annealing experiments.

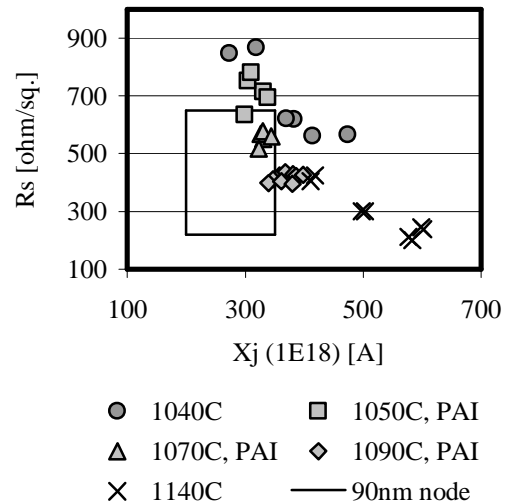


Figure 3: The Temperature effect for BF_2^+ implants.

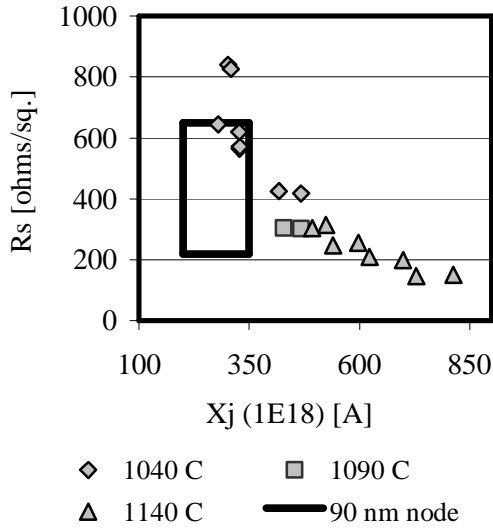


Figure 4: The Temperature effect for B^+ implants.

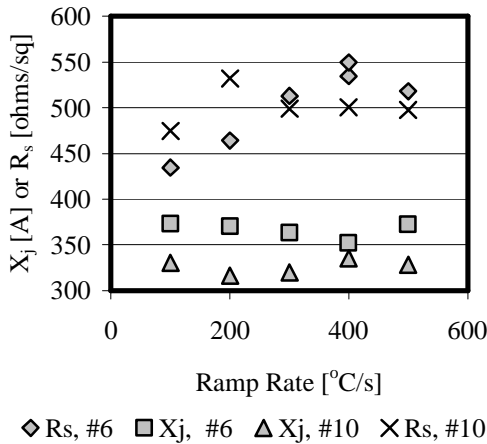


Figure 5: Effect of ramp-up rate on X_j and R_s values for two BF_2^+ implanted samples.

The effects of temperature and ramp rate can be predicted by the amount of thermal energy seen by the sample. This amount of thermal energy, or the thermal budget, can be quantified in terms of a diffusion distance, which is calculated by the integration of the Arrhenius equation over time. The integral is given by Equation 1.

$$\text{Thermal Budget} = D_o \int \exp\left(\frac{-E_a}{k_b T}\right) dt \quad [1]$$

where D_o and E_a are the pre-exponential diffusion constants and activation energies, respectively. These constants are unique to implant species and differ for dopant activation and diffusive motion. Therefore, an optimized thermal budget, which is primarily controlled by peak temperature, can be found. The area under the temperature-time profile, within $50^{\circ}C$ of the peak, is increased drastically by increasing the spike temperature, but the effect on the integral is only slight for changes in only the upward slope. Thus, the ramp-up rate effect on the X_j/R_s values is small. The control of the junction depth by the thermal budget is illustrated in Figure 6. The graph shows the relation of measured implant depth to the calculated thermal budget for BF_2^+ implants.

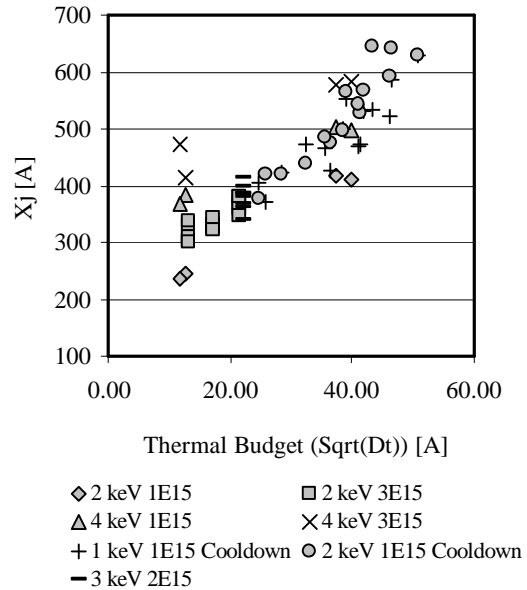


Figure 6: Relation of measured implant depth to the calculated thermal budget for BF_2^+ implants.

Figures 7 and 8 separate the effects of implant energy and dose for B^+ implants. As expected, decreasing the implant dose and energy decreases the junction depth. The sheet resistance is decreased by increasing the implant dose and energy. Thus, there is and obvious

trade-off between the two measurements of junction quality.

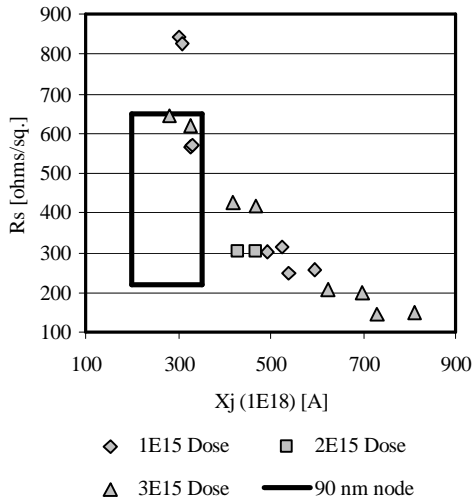


Figure 7: Effect of implant dose for B⁺ implants.

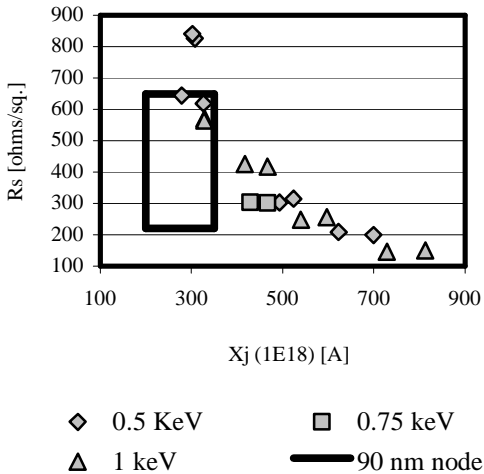


Figure 8: Effect of implant energy for B⁺ implants.

However, Ge PAI implants allow a decrease in junction depth without sacrificing the percentage of dopant activation. This trend is revealed, for BF₂⁺ implants by Figure 9. One can see that the curve is shifted slightly to the lower right of the X_j/R_s values without PAI. The implants are separated by PAI dose in this figure.

The annealing of the source/drain junctions served another function, in addition to activating the dopant⁶. Defects in the Si crystal, introduced by ion implantation, must be repaired. Implant damage will increase junction leakage. Transmission electron microscopy revealed no defects for the five samples cross-sectioned. The chosen samples are italicized in Table I. This proves that the defect size is less than 30 Å, and the defect density is less than 1E7/cm². Typically defects are eliminated by anneals above 850°C. Our results indicate that this spike annealing process is not an exception. Junction leakage is not expected to be a problem for transistors fabricated in this manner.

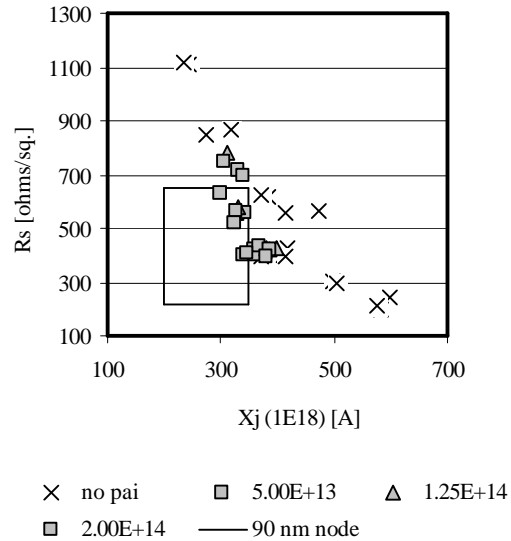


Figure 9: Effect of Ge pre-amorphization for BF₂⁺ implants. Points separated by PAI implant dose.

CONCLUSION

Low-energy boron implants activated by a very sharp spike anneal can be used to obtain the X_j/R_s requirements specified by the International Technology Roadmap for Semiconductors for the 90nm technology node. There is a compromise of the fraction of activated dopant when the effective annealing time is decreased simply by increasing ramp rates. When all influencing parameters are optimized spike annealing represents a means to achieve low sheet resistance and a shallow junction depth. The experimental conditions used for blanket wafer measurements may be duplicated in order

to produce ultrashallow junctions in p^+ transistors.

REFERENCES

- [1] *International Technology Roadmap for Semiconductors – Front End Processes*, Semiconductor Industry Association, p. 124, 1999
- [2] A. Agarwal, H-J Gossman, and A.T. Fiory, *Mat. Res. Soc. Symp. Proc.*, vol. 568 (1999) p. 19
- [3] E.J.H Collart et al., *Proceeding of the USJ Conf.*, p. 48, 1997
- [4] A. Jain, *Proc. of the Elec. Chem. Soc.* 2000
- [5] A.T. Fiory, and K.K. Bourdelle, *Appl. Phys. Lett.*, vol. 74 (1999), p. 2658
- [6] K.S. Jones and G.A. Rozgonyi, “Extended Defects from Ion Implantation and Annealing,” in *Rapid Thermal Processing*, R.B. Fair Ed. , Academic Press Inc. 1993